Higher-order contributions observed in three-dimensional $(e,2e)$ cross-section measurements at 1-keV impact energy

M. Dürr,[1] C. Dimopoulou,[1,2] B. Najjari,[1] A. Dorn,[1] K. Bartschat,[3] I. Bray,[4] D. V. Fursa,[4] Zhangjin Chen,[5,*] D. H. Madison,[5] and J. Ullrich[1]

[1]*Max-Planck-Institut für Kernphysik, Saupfercheckweg 1, 69117 Heidelberg, Germany*

[2]*Gesellschaft für Schwerionenforschung, Planckstrasse 1, 64291 Darmstadt, Germany*

[3]*Department of Physics and Astronomy, Drake University, Des Moines, Iowa 50311, USA*

[4]*ARC Centre for Antimatter-Matter Studies, Curtin University, Perth, WA 6845, Australia*

[5]*Laboratory of Atomic and Molecular Research, University of Missouri-Rolla, Rolla, Missouri 65409, USA*

We present experimental and theoretical fully differential cross sections for single ionization by fast, 1-keV (v=8.6 a.u.) electron impact. The cross sections were measured using a momentum imaging technique for electrons and ions (reaction microscope), which covers a large fraction of the emission angles for emitted low-energy electrons ($E<15$ eV) and a wide range of scattering angles. Therefore comprehensive data sets are obtained for ionizing collisions at small relative momentum and energy transfer from the projectile to the target system. The experimental data are compared with predictions from several state-of-the-art theoretical calculations. At this high impact energy the calculated cross section for electron emission out of the scattering plane appears to be particularly sensitive to the treatment of higher orders in the projectile-target interaction within perturbative models.

I. INTRODUCTION

Kinematically complete experiments on single ionization of atoms serve as a powerful method for the investigation of the dynamics of quantum mechanical few-body systems. For electron impact, in particular, the so-called $(e,2e)$ studies determine the momentum vectors of all continuum particles, thereby allowing for stringent tests of theoretical models for all kinematical situations that are experimentally accessible. As a consequence, enormous progress in the theoretical treatment of single ionization has been achieved in the past decade. In particular, the most fundamental three-body breakup system, electron-impact ionization of atomic hydrogen, was solved within the numerical accuracy [1] for projectile energies a few eV above the ionization threshold. For helium where the collision dynamics involves four interacting Coulomb particles, this goal is far from being reached. Nevertheless, the most advanced theories succeeded in reproducing well the available experimental multiply differential cross sections in both shape and absolute scale (see, for example, Refs. [2–4]).

However, strong and puzzling discrepancies with state-of-the-art theoretical predictions were observed in single ionization of helium by fast charged particles, first for ionic projectiles (100 MeV/amu C^{6+}) [5] and subsequently, also for electron impact [6]. These deviations were uncovered by applying a novel multiparticle imaging technique for the secondary ions and electrons, the so-called reaction microscope [7], which allowed one to cover essentially the entire solid angle for detection of both the ejected electron and the residual ion. Hence, the fully differential cross section (FDCS) could be measured for nearly all geometrical situations and,

for the first time, a complete image for emission of low-energy electrons from helium in singly ionizing collisions by charged particle impact could be provided, covering a large fraction of the full solid angle and a range of energy and momentum transfers.

For collisions at small momentum and energy transfer to the target, discrepancies between experimental data and theoretical predictions were most pronounced in the particular case when the initially bound electron was emitted *out* of the scattering plane determined by the incoming and outgoing projectile momentum vectors $\mathbf{k}_0$ and $\mathbf{k}_1$, respectively. (The ejected electron momentum is defined $\mathbf{k}_2$). For electron emission in the scattering plane, on the other hand, good agreement between experiment and theory was found where at higher impact energies, in particular, perturbative treatments appeared to describe the collision dynamics sufficiently accurate to obtain good agreement with the experimental data [8]. On the other hand, the noncoplanar cross section for such collisions with low energy and momentum transfer has, to date, been poorly explored using "conventional" $(e,2e)$ spectrometers, and most out-of-plane data were obtained at low impact energies [4,9–12].

In this sense, the application of the momentum imaging technique to study $(e,2e)$ processes with helium represents a major step forward, since the reaction microscope obtains comprehensive and consistent data sets over a large range of collision geometries [6]. The latter is effectively impossible with the conventional technique because of the challengingly low count rates. In fact, the three-dimensional cross-section images obtained with the reaction microscope at two different impact energies, $E_0=102$ eV and $E_0=1$ keV, revealed a significant enhancement of the out-of-plane emission [6]. This result is in striking and surprising disagreement with the theoretical three-Coulomb (3C) model presented in the work by Brauner, Briggs, and Klar [13], which includes the correlation of the three-body final-state continuum and almost per-

*Present address: Kansas State University, Manhattan, Kansas 66506-2604, USA.

fectly described the cross section in the extensively investigated scattering plane at impact energies as high as 600 eV [14,15]. While the observed out-of-plane features apparently stem from higher orders in the projectile-target interaction, the reason for the failure of the 3C model, which accounts for such higher-order contributions, remained unclear.

At the lower electron-impact energy of $E_0 = 102$ eV, the out-of-plane cross sections obtained with the reaction microscope were compared with predictions from various theoretical models [16]: the three-Coulomb-wave approach (3C), two second-order distorted-wave models, and the nonperturbative CCC model based on a close-coupling expansion of the multielectron wave function. Since the CCC approach fully accounts for the mutual correlations, it was the only one to achieve good agreement for all considered scattering geometries at this low impact energy. As mentioned above, the 3C model failed drastically out of plane, whereas the distorted-wave methods reproduced the data. However, since the correlations between the projectile, the recoil ion, and the ejected electron are inseparable at this low impact energy, no definite conclusion could be drawn regarding which particular ingredient of the distorted-wave models was crucial to correctly describe the out-of-plane features.

At the high impact energy of 1 keV considered in the present work, methods that treat the interaction between the projectile and the target within a perturbative expansion, such as the well-known Born series, are generally expected to provide an accurate description of the collision process, as was indeed demonstrated for the FDCS in the scattering plane [17]. Thus, the coupling between the projectile and the target can be considered as weak. Collisions with strongly asymmetric energy sharing between a fast scattered projectile and a slowly ejected electron are of major relevance, since they strongly dominate the total cross section. For this situation, the basic features in the FDCS as a function of the ejection angle are correctly predicted by the first Born approximation (FBA) and can be summarized as follows: the scattering plane is characterized by the well-known binary or recoil double-lobe structure and the FDCS is axially symmetric with respect to the momentum transfer axis $\mathbf{q}$. Correspondingly, the cross section in the plane perpendicular to $\mathbf{q}$ exhibits an isotropic angular dependence. Signatures of higher-order effects in the projectile-target interaction are a change in the ratio of binary-to-recoil peak intensity and a deviation from axial symmetry with respect to $\mathbf{q}$, i.e., an angular shift of the peak positions (see, for example, Ref. [18]) or shape deviations from cylindrical symmetry. The symmetry properties of the cross section can be studied in detail using the 3D images obtained with the reaction microscopes. The electron emission in the plane perpendicular to the scattering plane exhibits a particularly high sensitivity to higher-order contributions, since the first-order contributions themselves are weak.

The qualitative effect of higher-order processes on the cross section perpendicular to $\mathbf{q}$ was also demonstrated in a theoretical study [19] sparked by the 100 MeV/u ion impact results, where the anisotropy of the cross section in the plane perpendicular to $\mathbf{q}$ was shown to be the result of higher orders in the projectile-target interaction. Specifically, an enhancement for electron emission perpendicular to the scatter-

ing plane for negatively charged particles while a reduction was predicted for positively charged ions.

In a previous publication [6] we showed that the anisotropy of the noncoplanar cross section for the 1-keV electron-impact ionization of He—leading to an enhanced out-of-plane emission—is qualitatively reproduced by the 3C model, although it underestimates the magnitude of the cross section by a factor of 2. This observation coincides with the observation in ion impact, where so far all models, including the projectile-target interaction up to second or higher orders in perturbation theory [19], fail to describe the ion-impact data out of plane. For electron impact the out-of-plane enhancement observed in the noncoplanar FDCS in single ionization of Mg by fast electrons (400–3000 eV) recently reported in [20] was interpreted as an additional elastic scattering of the projectile from the residual ion. In a further theoretical study by Foster *et al.* [21] on the recent Mg out-of-plane data, it was demonstrated that the noncoplanar scattering geometry sensitively reacts to the details of the description of the projectile–residual-ion interaction. For the Mg target, a refined description with distorted waves calculated in the properly screened potential of the nucleus greatly improves the agreement with the experimental data over the 3C model, which uses a simple Coulomb wave for the projectile.

The limitations of computational resources currently prohibit the application of distorted-wave models to fast and heavy projectiles. Hence the question whether the interpretation of Foster *et al.* is true remains open for 100 MeV/u C^{6+} ion impact. In a recent publication Harris *et al.* [22] studied the influence of electron exchange between the ejected and the residual bound electron for ion impact and found that accounting for it insignificantly changes the theoretical FDCS results. Therefore this physical effect, which was previously unaccounted for in computational models, may be excluded as an explanation for the observed discrepancies.

In this paper we present a systematical study of the FDCS for 1-keV electron impact under asymmetric collision kinematics, i.e., at small energy and momentum transfer. Our particular focus is on the out-of-plane cross section, where the electron emission perpendicular to the momentum transfer directions serves as a particularly sensitive probe of higher-order projectile target interactions. The *absolute* experimental data, *independently* normalized to the generalized oscillator strength, are compared with predictions from diverse theoretical approaches based on perturbative treatments: the 3C model, a hybrid first-order and second-order plane-wave Born approximation for the projectile combined with a convergent R matrix (close-coupling) description of the ejected-electron–residual-ion interaction (PWB1-RMPS and PWB2-RMPS), as well as a first-order and second-order distorted-wave model for the projectile and the ejected electron (DWB1 and DWB2). Furthermore, we test to what extent the fully nonperturbative convergent close-coupling (CCC) method within its single active electron approximation succeeds in describing the fine details of the experimental data. Finally, instrumental effects were systematically studied by convoluting the instrumental function by means of a Monte Carlo simulation as presented in [23].
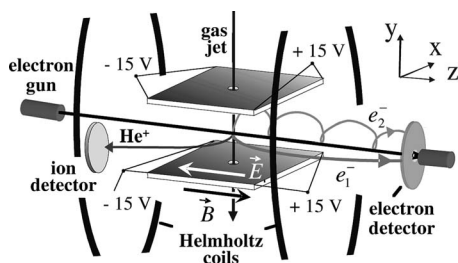
FIG. 1. Schematic view of the experimental setup.

II. EXPERIMENT

The complete details of the ionizing collision are explored by a multielectron recoil-ion momentum spectrometer (reaction microscope), which will be briefly described in the present chapter. A well-focused (1 mm FWHM), pulsed electron beam (pulse length 1.5 ns FWHM, repetition rate= 200 kHz, 10^4 electrons/pulse)—produced by a thermocathode gun—crosses and ionizes a supersonic helium jet (2 mm diam, 10^{12} atoms/cm^3). The fragments of the ionized He atom, i.e., the ejected electron and the recoiling He$^+$ ion, are extracted into opposite directions by a weak uniform electric field (typically 2 V/cm) over 11 cm. After extraction, the electron and the ion pass through a field-free drift region of 22 cm and are detected by two time- and position-sensitive multihit detectors. A uniform magnetic field of 10.8 G is applied parallel to the direction of the extraction field to confine the electron motion transverse to the electric field, thereby preventing electrons from hitting the field electrodes before reaching the detector. With this projection technique, a large part of the full solid angle is covered, essentially 100% for the detection of target ions and 80% for the detection of electrons below 20 eV. From the hitting positions and the time of flight, the vector momenta of the particles can be calculated. A detailed discussion of the imaging technique can be found in [24].

Different from all previous designs reported in [7,25], the reaction microscope dedicated to electron-impact ionization experiments was modified by aligning the electron projectile beam exactly parallel to the electric and magnetic extraction fields, into the target, and further on to the forward electron detector (see Fig. 1). In order to avoid the complete saturation of the electron detector by the unscattered projectiles (10^8/s), a central bore (5 mm diam) in the MCP stack is required to allow for their passage. In this way, unscattered electrons are collected on the delay line behind the bore of the detector and degradation of the sensitive detector plates, as well as high background due to backscattering of projectiles, is avoided.

The projectile beam follows the collinear trajectory, independent of the adjusted beam energy and the strength of the extraction fields. Hence, in contrast to the previous setup, electron-impact ionization experiments at low-impact energies become feasible with the reaction microscope [6,16]. For single-ionization experiments, the new setup enables the detection of the scattered projectile and the deduction of its scattering angle with a better resolution than in a typical ion-impact experiment, where the projectile scattering angle

is reconstructed from the target momenta via momentum conservation. As a result, our $(e,2e)$ experiment overcomes the major drawback of kinematically complete ion-impact experiments, in which the thermal motion in the molecular target beam determines the achievable resolution. Even though target temperatures as low as 1 K are routinely achieved in supersonic jets, the detection of the scattered projectile in our experiment allows for the resolution of the momentum transfer by a factor of 2–3 better than in previous ion-impact experiments.

In our experiment we use the following Cartesian coordinate system: The projectile beam propagation, which is aligned along the electric extraction field, defines the z axis, the y direction is oriented along the target beam, and the x axis is transverse to both of them (see Fig. 1). The z axis is sometimes referred to as the spectrometer axis. However, for the discussion of the imaging properties of our spectrometer, we express the vector momentum of the electron using cylindrical coordinates $\mathbf{k}=(k_{\parallel},k_{\perp},\varphi)$ taking into account the symmetry with respect to the projectile axis: The projectile beam propagation, which is aligned along the electric extraction field, defines the longitudinal direction $k_{\parallel}=k_z$. The magnitude of the electron momentum transverse to the projectile beam is $k_{\perp}=\sqrt{(k_x)^2+(k_y)^2}$. The azimuthal angle φ $=\arctan(k_y/k_x)$ describes the emission angle in the plane perpendicular to the projectile beam axis.

The longitudinal momentum component is obtained in a straightforward way from the electron's time of flight. The transverse motion is somewhat more difficult, because the additional magnetic field forces the electrons onto a spiraling motion, which they start at the crossing point on the projectile beam axis. The transverse components $k_{\perp}$ and φ are reconstructed from the detector position by tracing back the trajectory to the crossing point, where additional information regarding the fraction of traversed cyclotron turns $\alpha=\omega t$ (ω: cyclotron frequency, t: time-of-flight) upon the arrival of the electron at the detector is needed. This implies the knowledge of the magnetic field strength with sufficient accuracy, which is given in the present experiment. When the electrons have completed an integer number of n cyclotron turns (n $=0,1,2,\dots$) they are focused back to the spectrometer axis irrespectively of their transverse momentum $\mathbf{k}_{\perp}$. This results in a node for the electron detector position at flight times of $n\times 2\pi/\omega$. In between such nodes, the electrons on the other hand have reached the largest radial distance from the spectrometer axis, such that the position information at these times yields the transverse-momentum components with an optimal resolution.

The size of the detector and the strength of the magnetic field determine the range of accepted electron momenta. For the data presented in this paper, the scattered projectile electrons were detected together with ejected electrons having transverse momenta in the range $0.3<k_{\perp}<1.6$ a.u., and also with the residual ion. Although such a triple coincidence of all final-state continuum particles is not necessary in order to obtain the complete kinematic information about the collision process, it delivers superior background suppression. The electron momentum resolution depends upon how well the time and position of the ionizing collision can be determined and, therefore, on the temporal pulse width and the

focus diameter of the projectile beam in the target. For the focus diameter of 1 mm and the pulse length of 1.5 ns, the transversal momentum resolution of the electrons is estimated to be better than $\Delta k_\perp < 0.1$ a.u.

The longitudinal resolution depends upon the time of flight of the electrons, and thus, on the longitudinal momentum itself. For slow electrons with energies of a few eV, the relative uncertainty resulting from the timing resolution leads to an estimated value of $\Delta k_\parallel < 0.02$ a.u. However, for asymmetric collisions in an experiment, in which only a small fraction of the projectile energy and momentum is transferred to the target studied, the longitudinal momentum $k_{1,\parallel}$ of the high-energy scattered projectile cannot be resolved due to its large velocity. Thus the extraction of the momentum transfer through $q_\parallel = k_{0,\parallel} - k_{1,\parallel}$ is not viable. However, the longitudinal momentum transfer is extracted through its approximative relation to the energy transfer to the target by $q_\parallel = (E_e + V_{ion})/v_P$ (E_e: ejected electron energy, V_{ion}: ionization potential) from the measured ejected-electron momentum.

The momentum transfer transverse to the incoming beam direction $\mathbf{q}_\perp$ can be deduced from the transverse momentum $\mathbf{k}_{1,\perp} = (k_{1,x}, k_{1,y})$ of the scattered projectile after it is deflected from the incoming beam axis. The resolution of this component was optimized by setting the strength of the magnetic field to a value such that the fast projectiles complete a half cycle of the cyclotron motion on their way from the interaction zone to the detector. In this way, the relative influence of uncertainties due to limited position and time resolution is minimized. This results in the optimal resolution for the momentum transfer.

Absolute normalization of data

The absolute normalization of the cross sections is performed exploiting the wide range of scattering angles recorded in a single run of the experiment by extrapolating the generalized oscillator strength (GOS) to the optical limit. Following the procedure reported in [26], a polynomial function is used for a controlled extrapolation of the GOS to zero momentum transfer. The extrapolated result is scaled to the total ionization cross section by absorption of a single photon, which was published with an accuracy of better than 3% by Samson *et al.* [27]. This method has been critically discussed in [28] where it was concluded that it delivers a reliable normalization. The uncertainty in determining the absolute scale depends critically upon the lowest measurable momentum transfer. Here the final limit for the zero scattering angle is imposed by the inelasticity of the collision, which amounts approximately to $q_{min} \approx (E_e + V_{ion})/v_P$. In our $(e, 2e)$ experiment the limitations lie in the lowest transverse-momentum acceptance of the scattered projectile, $q_\perp \gtrsim 0.4$ a.u. or $\theta_1 \gtrsim 2.7°$, respectively. The experimental GOS was evaluated for the ejected electron energy of $E_e = (5 \pm 1)$ eV as a function of momentum transfer with a binsize of ± 0.05 a.u. In particular, towards small momentum transfers the cross section rises steeply (approximately by $1/q^4$) and the experimental GOS may be strongly affected by the binning or the experimental resolution. We therefore

cross-checked our data in a comparison with very similar data reported at slightly different energy of the ejected electron and no significant deviations were observed [29]. From our fitting procedure, we obtained the uncertainty of the absolute scale to less than 15%.

III. THEORY

The various theoretical models have been described in our previous paper [16] for 102 eV electron impact, where additional references to the original papers were provided as well. Hence, we will only briefly summarize the key ideas behind the various approaches.

To begin with, the three-Coulomb (3C) wave-function approach introduced in [13] is built upon a perturbative treatment, but it accounts asymptotically for high-order effects in the final-state between the two continuum electrons and the residual ion. We performed calculations with and without taking into account exchange between the two final-state continuum electrons and found it to be unimportant in the present asymmetric energy sharing kinematics. The 3C results shown below were obtained without including exchange effects.

The strength of distorted-wave models lies in the fact that they account for more of the short-range physics, i.e., the actual ionization process, than the 3C approach, at the cost of neglecting the correct asymptotic boundary conditions. Specifically, we present below first-order (DWB1) and second-order (DWB2) results obtained as described by Chen and Madison [30]. In these models, the projectile and the ejected electron are described by distorted waves calculated in the static potential of the neutral atom (projectile) and the residual ion (ejected electron). Exchange effects are neglected for the fast projectile and approximated by a local potential for the ejected electron. All channel-coupling effects are neglected as well, but the only approximations made in the evaluation of the second-order contribution to the ionization amplitude are the restriction that one of the target electrons in the intermediate states always has to be in the $1s$ orbital and that the continuum states are represented by a discrete sum over pseudostates.

Compared to the DBW1 and DWB2 methods, the DWB1-RMPS and DWB2-RMPS methods improve upon the treatment of both the initial target state and the ejected-electron–residual-ion interaction by using a convergent R matrix with pseudostates (RMPS) expansion for this part of the problem. Hence exchange and channel-coupling effects for the slow electron are treated numerically accurate and effectively convergent. The set of intermediate states in the second-order term also includes a large number of doubly excited states, but some additional approximations are necessary to make the evaluation of that term computationally feasible [31]. Below we show results obtained in plane-wave (PWB1-RMPS and PWB2-RMPS) hybrid methods, since distortion effects for the projectile are very small at 1-keV incident energy and hence the partial-wave expansion can be replaced by the analytic Bethe integral.

Finally, the convergent close-coupling (CCC) method treats the problem fully nonperturbatively. This was done
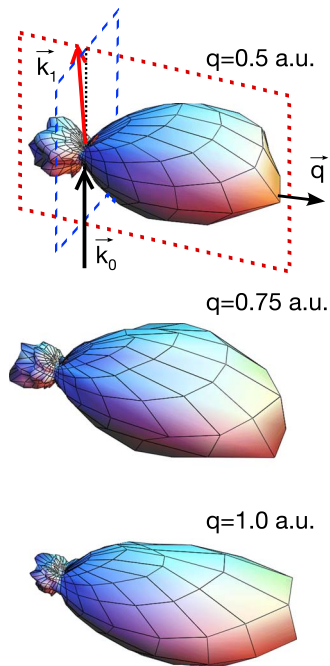
FIG. 2. (Color online) Fully differential cross sections for electron-impact single ionization of helium by 1-keV electrons presented as a three-dimensional polar plot at fixed energy of the ejected electron $E_2 = 10$ eV and three different momentum transfers q of 0.5, 0.75, and 1.0 a.u. For $q = 0.5$ a.u. the momentum vectors of the incoming projectile $\vec{k}_0$, the scattered projectile $\vec{k}_1$, and the momentum transfer $\vec{q}$ are indicated. These vectors define the projectile scattering plane (dotted frame). The plane perpendicular to the scattering plane which contains the incoming projectile momentum is indicated by a dashed frame.

both in the frozen-core approximation, where of the target electrons remains a spectator locked in the $1s$ orbital of He$^+$ and leading to a 0.84 eV error in the ionization potential, and a configuration expansion that reduces this error to approximately 0.1 eV. The difference between these two calculations was found to be negligible for the cross sections presented. The essential idea of the method is to calculate electron-impact excitation of positive-energy pseudostates, followed by a projection of the pseudostates onto true continuum functions. The latter projection allows for the expression of the true ionization amplitude as a linear combination of various excitation amplitudes with properly defined weights and hence the calculation of fully differential ionization cross sections.

IV. RESULTS AND DISCUSSION

In Fig. 2 the $(e, 2e)$ cross section is plotted as a three-dimensional polar plot representing the emission pattern for an ejected electron energy of $E_2 = 10$ eV and a momentum transfer fixed to three different values $q = (0.5 \pm 0.11)$ a.u., (0.75 ± 0.11) a.u., and (1.0 ± 0.2) a.u., corresponding to projectile scattering angles of $\theta_1 = 3.2°$, 5°, and 6.7°. The dominant dipolar pattern with the high intensity binary lobe along the direction of **q** and the recoil lobe in the direction of $-$**q** is
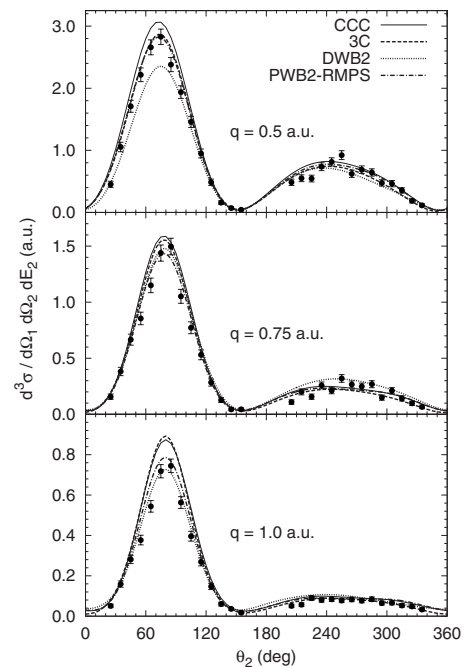

FIG. 3. Coplanar fully differential cross sections (in atomic units) for 1-keV electron-impact single ionization of helium for an ejected electron energy of $E_2 = 10$ eV and three different momentum transfers of 0.5, 0.75, and 1.0 a.u. Theoretical curves: CCC (solid lines), 3C (dashed lines), DWB2 (dotted lines), and PWB2-RMPS (dot-dashed lines).

clearly visible. The scattering plane and the perpendicular plane containing the incoming projectile axis are denoted by dotted and dashed lines, respectively. For better visibility the polar plots have been rescaled to the same magnitude of the binary peak. The emission pattern exhibits the well-known behavior, where the intensity of the recoil lobe decreases relative to the binary lobe with increasing momentum transfer. In this 3D representation a cross-section ridge in between the recoil and binary lobes is visible. It is pronounced for emission perpendicular to the projectile scattering plane, particularly for the largest momentum transfer of $q = 1$ a.u., where the cross-section magnitudes of the out-of-plane contribution and the recoil lobe are comparable.

For a detailed investigation of the cross sections and a quantitative comparison with theory, we consider the absolute cross section as a function of the emission angle of the ejected electron in the scattering plane (Fig. 3) and in the plane perpendicular to the scattering plane (Fig. 4). These cross sections correspond to cuts through the 3D representations of Fig. 2 within the planes marked by the dotted frame and the dashed frame, respectively. For the cross sections presented in the figure, electrons with emission angles of $\pm 10°$ above and below these planes were accepted in the experimental evaluation. The resulting cross sections are shown as a function of the angle θ_2 enclosed by the ejected-electron momentum and the projectile axis such that $0° \leq \theta_2 \leq 360°$.

In the scattering plane (Fig. 3) the agreement of theory and experiment is fairly satisfactory since the absolute magnitudes of the cross sections deviate by no more than 17%.
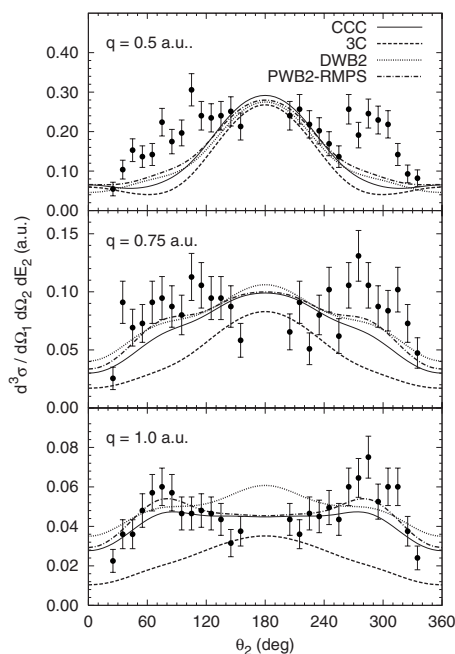
FIG. 4. Fully differential cross sections (in atomic units) in the plane perpendicular to the scattering plane for 1-keV electron-impact single ionization of helium for an ejected electron energy of $E_2 = 10$ eVand three different momentum transfers of 0.5, 0.75, and 1.0 a.u. Theoretical curves: CCC (solid lines), 3C (dashed lines), DWB2 (dotted lines), PWB2-RMPS (dot-dashed lines).

The PWB2-RMPS model (dash-dotted line) agrees very well for all three momentum transfers with regard to shape and magnitude. The 3C model (dashed line) and the CCC calculation (continuous line) overestimate the binary-peak intensity most visibly at a momentum transfer of $q = 1$ a.u. while the DWB2 model (dotted line) significantly underestimates the binary-peak intensity at the smallest momentum transfer of $q = 0.5$ a.u. It is likely that the principal reason for the success of the PWB2-RMPS model is its overall best description of the "structure part" of the problem, namely, the initial bound state and the ejected-electron–residual-ion interaction.

The situation is different in the plane perpendicular to the scattering plane. In this geometry, the experimental data for all three momentum transfers exhibit a trend of an enhanced cross section at 90° and 270°, i.e., for electron emission perpendicular to the scattering plane. This corresponds to the bulge in the 3D emission patterns discussed above. The relative intensity of the out-of-plane enhancement becomes larger with increasing momentum transfer, as was already observed in the 3D images of Fig. 2.

At $\theta_2 = 180°$ a fraction of the recoil-lobe intensity appears as a maximum in this cutting plane perpendicular to the scattering plane. This results firstly from the kinematical forward tilt of the momentum transfer vector, which is 79°, 85°, 87° with regard to the projectile forward direction for the three considered momentum transfers 0.5, 0.75, and 1 a.u. Secondly, as can be seen in Fig. 3, the width of the recoil lobe is larger ($\Delta\theta_2 \approx 200°$ between cross-section minima enclosing the recoil peak) than the width of the binary lobe ($\Delta\theta_2 \approx 160°$). In the panels of Figs. 2 and 3, both effects give rise

to cross-section minima in the projectile forward direction ($\theta_2 = 0°$) while at $\theta_2 = 180°$ a considerable fraction of the recoil peak intensity is visible. No experimental data points could be taken in close vicinity of these directions, since the apparatus has zero acceptance for electrons emitted in directions near the projectile axis due to the hole in the electron detector.

For the large momentum transfer case, $q = 1$ a.u., all theories except for the 3C model reproduce the out-of-plane maxima at emission angles $\theta_2 = 90°/270°$ in rather good agreement with experiment. The 3C model clearly fails by strongly underestimating the out-of-plane feature. The DWB2 model reveals a different discrepancy, namely, a considerably higher cross section compared to the PWB2-RMPS and CCC models with respect to the intensity at 180°. While there are no experimental values close to 180°, the trend of the available data points in the vicinity of the acceptance hole is clear: the data points from 135° to 155° and from 225° to 205°, respectively, are in contradiction to the DWB2 results while in good agreement with the CCC and PWB2-RMPS predictions.

For lower values of the momentum transfer, in particular, for $q = 0.5$ a.u., all models underestimate the magnitude of the cross-section enhancement perpendicular to the scattering plane. The PWB2-RMPS and DWB2 models qualitatively indicate such an enhancement as a weak hump at those specific angles, although missing the magnitude almost by a factor of 3. On the other hand, all four presented models reproduce the peak at 180° for $q = 0.5$ a.u., which is consistent with the good agreement for the recoil peak observed in the coplanar cross section.

The fact that the plane-wave hybrid model PWB2-RMPS reproduces the out-of-plane maxima, at least for $q = 0.75$ a.u. and $q = 1.0$ a.u., suggests some conclusions about their origin. According to the three-dimensional images of Fig. 2, these features exhibit no axial symmetry with respect to the momentum transfer direction. Since this symmetry is inherent in a first-order plane-wave Born model, the second-order contribution in the PWB2 model must give rise to these features.

In order to further elucidate this conclusion, we now consider electron emission in the plane perpendicular to the momentum transfer **q**, which, as mentioned above, is tilted 11°, 5°, and 3°, respectively, into the forward direction with respect to the transversal direction perpendicular to the incoming beam. The resulting cross section is plotted as a function of the emission angle θ' in Fig. 5. In the plane perpendicular to **q** this is the angle between the ejected electron momentum and the scattering plane. In this representation the out-of-plane enhancement results in pronounced maxima at 90° and 270°. As mentioned above, any first-order plane-wave treatment of the projectile-target interaction—in our case the PWB1-RMPS model—leads to a constant and therefore isotropic cross section, thereby reflecting the symmetry of the FBA with respect to the momentum transfer **q** (see Fig. 5). Changing the description of other parts of the problem, such as the initial state and the ejected-electron–residual-ion interaction, only affect the value of that constant.

Inclusion of the second-order contributions (PWB2-RMPS) apparently leads to the peak structures at 90° and
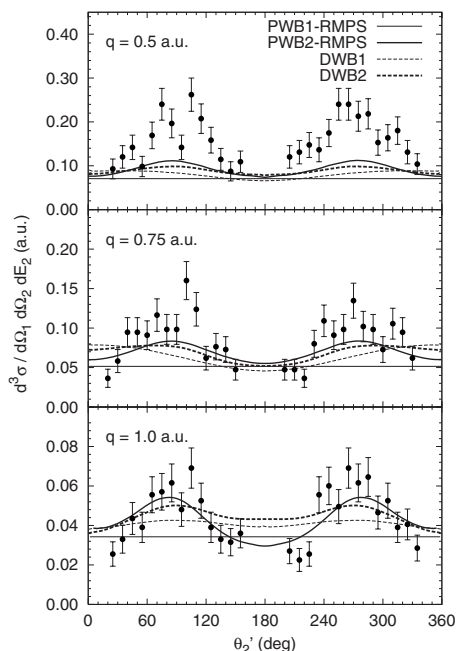
FIG. 5. Fully differential cross sections (in atomic units) in the plane perpendicular to the momentum transfer vector **q** for 1-keV electron-impact single ionization of helium for an ejected electron energy of $E_2 = 10$ eV and three different momentum transfers of 0.5, 0.75, and 1.0 a.u. Theoretical curves: PWB1-RMPS (thin solid lines), PWB2-RMPS (thick solid lines), DWB1 (thin dashed lines), and DWB2 (thick dashed lines).

270°. Since the DWB1 model already includes some higher-order contributions in the projectile-target interaction, it is not surprising that its predictions already deviate from a straight line. Using only the first-order amplitude, however, apparently underestimates the out-of-plane maxima and the agreement somewhat improves after inclusion of the second-order amplitude (DWB2). Nevertheless, the PWB2-RMPS predictions are clearly in better agreement with the experimental data at $q=1.0$ and $q=0.75$ a.u. than the DWB2 results. This suggests that the approximations made in the PWB2-RMPS regarding the evaluations of the second-order term are less severe than those made in DWB2 for that term, the initial state, and the ejected electron. Finally, neither model correctly predicts the intensity of the electron emission perpendicular to the scattering plane at $q=0.5$, although PWB2-RMPS comes closest.

Since the largest disagreement occurs at low momentum transfers, which corresponds to small projectile scattering angles, the out-of-plane maxima might result from the resolution of the reaction microscope. Indeed, such instrumental effects can considerably influence the measured signal, in particular, out of the scattering plane, where the cross section is low relative to the coplanar emission. This was demonstrated, for example, by Fiol *et al.* [32], who presented results from a calculation that was convoluted with the momentum transfer resolution stated in the ion-impact experimental papers.

A very detailed analysis of the effect of the instrumental function of the reaction microscope on differential cross-
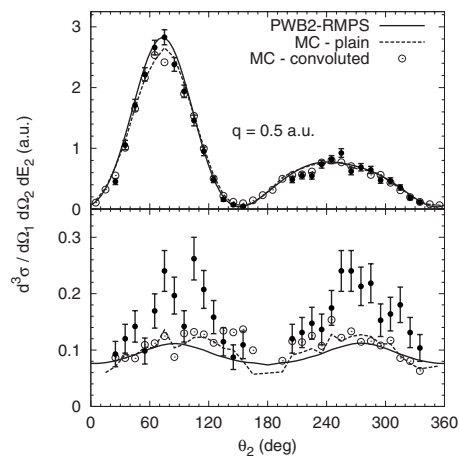

FIG. 6. Comparison of experimental and convoluted fully differential cross sections (in atomic units) in the scattering plane (top) and the plane perpendicular to the momentum transfer vector **q** (bottom) for 1-keV electron-impact single ionization of helium for an ejected electron energy of $E_2 = 10$ eV and a momentum transfer of 0.5 a.u. Theoretical curves: PWB2-RMPS (solid lines), Monte Carlo simulation results using the PWB2-RMPS results (dashed lines), and Monte Carlo simulation results convoluted with the experimental resolution (empty circles).

section measurements was recently presented for ion-impact cross-section data in [23]. In this case, the convolution includes the full complexity of the resolution by using the Monte Carlo simulation method. Briefly, in this procedure an event data file is artificially generated on the basis of a theoretical model, for example, a first Born approach, specifying the momenta of all final-state particles for each single-ionization event. The individual momentum components in the generated sample are then weighted by the theoretical results, such that the artificial event file provides a simulation of a real experiment. The error source is simulated by adding randomly selected contributions to each of the momentum components. These contributions follow a particular distribution, such that they provide an appropriate representation of the error source.

As mentioned in the experimental section, the reaction microscope used in our electron-impact ionization experiment allows for the detection of both the scattered projectile and the ejected electron. Thereby the technique becomes *independent of the target temperature*. This is not the case for kinematically complete studies of ion-impact ionization, where the recoil-ion momentum spectroscopy needs to be used to obtain the complete collision kinematics.

Consequently, a far superior resolution was achieved for the $(e,2e)$ data presented in the present paper. Nevertheless, in order to analyze the potential effect of the apparatus function and the statistics, we applied the Monte Carlo procedure presented in [23] to the present $(e,2e)$ results with 1 keV electrons. The event file was based upon the PWB2-RMPS model. From the event file, cross sections were extracted just as for the actual data and instrumental effects on the FDCS perpendicular to the momentum transfer were studied.

The results are shown in Fig. 6 for the smallest momentum transfer of 0.5 a.u., both in the scattering plane and in

the plane perpendicular to **q**. We found that the finite binning of the experimental cross section does not lead to any significant change in the evaluated experimental cross section. Furthermore, an effect on the measured FDCS out of the scattering plane was observed only by assuming an unrealistically poor resolution. Even then, this did not lead to pronounced cross-section maxima in the plane perpendicular to **q**. These findings suggest that the observed discrepancies at $q=0.5$ a.u. momentum transfer for the emission perpendicular to q are *not* the result of the instrumental resolution.

V. SUMMARY AND CONCLUSIONS

We have presented new experimental and theoretical results for fully differential cross sections for single ionization of helium by fast (1 keV) electron impact. A comparison of the experimental data, obtained for a large range of kinematical situations through a reaction microscope, with predictions from several state-of-the-art theoretical approaches, revealed good to excellent agreement for the dominant electron emission in the scattering plane. For emission out of the plane, on the other hand, only theories that describe the short-range part of the interaction in a somewhat sophisticated way—at the expense of neglecting the correct asymptotic boundary conditions—are able to reproduce the qualitative features seen in the experimental data. The side maxima seen in these data are not artifacts caused by an insufficient experimental resolution but are apparently due to second- or even higher-order effects in the projectile-target interaction. In addition to accounting for these effects in the description of the projectile, achieving quantitative agreement with experiment requires the use of highly sophisticated wave functions for the initial bound state and the ejected-electron–residual-ion interaction. Such quantitative agreement was indeed achieved for momentum transfers of 0.75 and 1.0 a.u., while some currently unresolved discrepancies remain for the smallest momentum transfer (0.5 a.u.) studied in the present experiment.

[1] T. N. Rescigno, M. Baertschy, W. A. Isaacs, and C. W. McCurdy, Science **286**, 2474 (1999).
[2] A. T. Stelbovics, I. Bray, D. V. Fursa, and K. Bartschat, Phys. Rev. A **71**, 052716 (2005).
[3] I. Bray and D. V. Fursa, Phys. Rev. A **54**, 2991 (1996).
[4] T. Rösel, J. Röder, L. Frost, K. Jung, H. Ehrhardt, S. Jones, and D. H. Madison, Phys. Rev. A **46**, 2539 (1992).
[5] M. Schulz, R. Moshammer, D. Fischer, H. Kollmus, D. H. Madison, S. Jones, and J. Ullrich, Nature (London) **422**, 48 (2003).
[6] M. Dürr, C. Dimopoulou, B. Najjari, A. Dorn, and J. Ullrich, Phys. Rev. Lett. **96**, 243202 (2006).
[7] J. Ullrich, R. Moshammer, A. Dorn, R. Dörner, L. P. H. Schmidt, and H. Schmidt-Böcking, Rep. Prog. Phys. **66**, 1463 (2003).
[8] H. Ehrhardt, K. Jung, G. Knoth, and P. Schlemmer, Z. Phys. D: At., Mol. Clusters **1**, 3 (1986).
[9] A. J. Murray and F. H. Read, Phys. Rev. Lett. **69**, 2912 (1992).
[10] A. J. Murray and F. H. Read, J. Phys. B **26**, L359 (1993).
[11] A. J. Murray, M. B. J. Woolf, and F. H. Read, J. Phys. B **25**, 3021 (1992).
[12] E. C. Beaty, K. H. Hesselbacher, S. P. Hong, and J. H. Moore, Phys. Rev. A **17**, 1592 (1978).
[13] M. Brauner, J. S. Briggs, and H. Klar, J. Phys. B **22**, 2265 (1989).
[14] M. Brauner, J. S. Briggs, and J. T. Broad, J. Phys. B **24**, 287 (1991).
[15] A. Franz and P. L. Altick, J. Phys. B **25**, 1577 (1992).
[16] M. Dürr, C. Dimopoulou, A. Dorn, B. Najjari, I. Bray, D. V. Fursa, Z. J. Chen, D. H. Madison, K. Bartschat, and J. Ullrich, J. Phys. B **39**, 4097 (2006).
[17] L. Avaldi, R. Camilloni, E. Fainelli, G. Stefani, A. Franz, H. Klar, and I. E. McCarthy, J. Phys. B **20**, 5827 (1987).
[18] H. Ehrhardt, M. Fischer, K. Jung, F. W. Byron, C. J. Joachain, and B. Piraux, Phys. Rev. Lett. **48**, 1807 (1982).
[19] A. B. Voitkiv, B. Najjari, and J. Ullrich, J. Phys. B **36**, 2591 (2003).
[20] R. W. van Boeyen, N. Watanabe, J. W. Cooper, J. P. Doering, J. H. Moore, and M. A. Coplan, Phys. Rev. A **73**, 032703 (2006).
[21] M. Foster, J. L. Peacher, M. Schulz, D. H. Madison, Z. J. Chen, and H. R. J. Walters, Phys. Rev. Lett. **97**, 093202 (2006).
[22] A. L. Harris, D. H. Madison, J. L. Peacher, M. Foster, K. Bartschat, and H. P. Saha, Phys. Rev. A **75**, 032718 (2007).
[23] M. Dürr, B. Najjari, M. Schulz, A. Dorn, R. Moshammer, A. B. Voitkiv, and J. Ullrich, Phys. Rev. A **75**, 062708 (2007).
[24] R. Moshammer, M. Unverzagt, W. Schmitt, J. Ullrich, and H. Schmidt-Böcking, Nucl. Instrum. Methods Phys. Res. B **108**, 425 (1996).
[25] A. Dorn, A. Kheifets, C. D. Schroter, B. Najjari, C. Hohr, R. Moshammer, and J. Ullrich, Phys. Rev. A **65**, 032709 (2002).
[26] K. Jung, R. Müller-Fiedler, P. Schlemmer, H. Ehrhardt, and H. Klar, J. Phys. B **18**, 2955 (1985).
[27] J. A. R. Samson and W. C. Stolte, J. Electron Spectrosc. Relat. Phenom. **123**, 265 (2002).
[28] A. Lahmam-Bennani, M. Cherid, and A. Duguet, J. Phys. B **20**, 2531 (1987).
[29] A. Duguet, M. Cherid, A. Lahmam-Bennani, A. Franz, and H. Klar, J. Phys. B **20**, 6145 (1987).
[30] Z. J. Chen and D. H. Madison, J. Phys. B **38**, 4195 (2005).
[31] R. H. G. Reid, K. Bartschat, and A. Raeker, J. Phys. B **31**, 563 (1998); (corrigendum) **33**, 5261 (2000).
[32] J. Fiol, S. Otranto, and R. E. Olson, J. Phys. B **39**, L285 (2006).